EARTHQUAKE ENGINEERING AND STRUCTURAL DYNAMICS, VOL. 25, 1177–1194 (1996)

RESPONSE OF EARTH DAMS TO P AND SV WAVES USING COUPLED FE-BE FORMULATION

HASSAN ABOUSEEDA* AND PANOS DAKOULAS†

Civil Engineering Department MS 318, Rice University, 6100 South Main, Houston, TX 77005-1892, U.S.A.

SUMMARY

A study of the effects of dam–foundation interaction on the response of earth dams to obliquely incident P and SV waves is presented. Emphasis is placed on the effects of the foundation flexibility and the spatial variability of the ground motion. The study is based on a rigorous hybrid numerical formulation that combines the efficiency and versatility of the Finite Element Method (FEM) and the ability of Boundary Element Method (BEM) to account for the radiation conditions at the far field. The developed hybrid method is very powerful and can be used efficiently to obtain accurate solutions of problems of complex geometry, material heterogeneity and, for time-domain analyses, material nonlinearity. The 2-D frequency-domain formulation is used here to investigate the response of infinitely long earth dams to obliquely incident P and SV waves. By accounting rigorously for the energy radiated back into the half-space, the study demonstrates the dramatic effect of the flexibility of the foundation rock in reducing the overall response of the dam. The effects of the spatial variability of the ground motion for P and SV waves travelling across the width of the dam are also important, but somewhat less pronounced than those of the foundation flexibility.

KEY WORDS: earth dams; wave propagation; soil–structure interaction; boundary element method; finite element method; dynamic response

INTRODUCTION

The seismic response of earth and rockfill dams has been the subject of considerable research in the last 20 years with primary focus on the effects of such factors as the dam and canyon geometries, the inhomogeneity of the dam material, the non-linear and inelastic behaviour of the material, the relative flexibility of the dam and the canyon or foundation materials, and, to only a limited extent, the spatial variability of the excitation. Detailed accounts of past contributions are available in two state-of-the-art reports by Gazetas[1] and Gazetas and Dakoulas.[2]

Previous numerical and theoretical studies on the effects of the spatial variability of the ground motion were limited by restricting simplifying assumptions. Early finite element studies[3,4] investigated the lateral response of long dams subjected to waves travelling across the dam width, but with no account of the effects of the dam–foundation interaction. These studies revealed that the response of a dam to a spatially variable motion may be substantially higher than that obtained for a space-invariant motion. Some results on the combined effects of wave passage and dam–canyon interaction have been presented using the Boundary Integral Equation Method,[5] but they are based on substantial idealization/simplification of the dam-canyon geometry. Recently, Dakoulas and his co-workers[6–9] presented a series of closed-form solutions using generalized shear beam models for dams built in canyons of semicircular, semielliptical and rectangular shapes and excited by obliquely incident SH waves propagating along the longitudinal direction of the dam. These solutions account either rigorously[6–8] or approximately[9] for the dam–canyon interaction effects, as well as for the wave scattering and diffraction phenomena associated with the presence of the dam-filled canyon. The results from these models demonstrate consistently the dramatic effect of the impedance ratio on

*Graduate Student
†Associate Professor

CCC 0098-8847/96/111177–18

Received 26 September 1995
Revised 16 April 1996

the dam response. They also show that obliquely incident waves impinging on the dam–canyon interface induce new vibrational modes in addition to those excited by uniform synchronous base motion. (For the symmetric dams and the waves examined,[6-8] the additional modes are antisymmetric.) Even at small incidence angles, the excitation of these modes may lead to substantially higher response in the dam than that caused by vertically propagating waves.

Given the importance of the base flexibility and the spatial variability of the ground motion, as clearly demonstrated in the aforementioned studies,[2-9] it is of interest to use a rigorous numerical formulation to conduct a comprehensive study of the effects of SV, P and Rayleigh waves travelling across the width and along the length of the dam.

The FEM, combined with transmitting boundaries or infinite elements, and the BEM have been used extensively to study soil–structure interaction and wave propagation problems. The FEM has been proven very efficient and versatile for finite-size problems, due to its effective handling of arbitrary geometry and material heterogeneity and non-linearity. However, several previously suggested modifications for handling infinite-domain dynamic problems seem to be either computationally expensive or have serious limitations. On the other hand, the BEM seems to be ideal for treating infinite domains, as it can inherently account for the radiation conditions at the far field, but it is less effective for treating heterogeneous materials and non-linear problems. To benefit from the advantages and avoid the limitations of the two methods, a hybrid FE–BE method has been developed,[10-12] which, with the recent substantial increase in computational power, is becoming more popular for problems of complex geometry, material heterogeneity and nonlinearity in the near field. The frequency-domain formulation of the hybrid FE–BE method has been used to study 2D and 3D soil–structure interaction problems,[13-15] the response of alluvial valleys,[16,17] wave scattering by surface irregularities[18] and other applications. Transient soil–structure interaction problems were also treated in the time domain to study the response of foundations, trenches and tunnels.[19-21]

To study the response of earth dams to travelling waves along any direction, a rigorous hybrid FE–BE formulation has been developed for general soil–structure interaction problems.[22] The two-dimensional frequency-domain formulation is used here to investigate the response of long dams to SV and P waves travelling across the width of the dam, assuming linear hysteretic soil behaviour. The case of Rayleigh waves will be presented elsewhere.

A concise description of the hybrid FE–BE formulation is given below. More details about the method may be found in Reference 22.

FORMULATION

Finite element method

Figure 1 presents the cross-section of a plane strain dam resting an elastic half-space. The dam body (finite domain) is discretized with finite elements. The displacement vector at point x within an element is approximated using shape functions, $u(x, \tau) = N\hat{u}(\tau)$, where N is the shape function vector and $\hat{u}(\tau)$ are the nodal displacement vector at time τ. The discretization error is minimized using the Galerkin weighted residual formulation,[23] in which the weighting function is taken the same as the shape function. The discretization renders the following matrix differential equation:

$$[M]\ddot{u} + [K]u + f = 0 \tag{1}$$

where $[M]$, $[K]$ are the global mass and stiffness matrices and f is the vector of nodal loads. For steady-state harmonic response, the nodal displacements can be expressed as $u = u(x)e^{i\omega\tau}$ which substituted in equation (1) leads to

$$[A]u = f \tag{2}$$

where

$$[A] = -\omega^2[M] + (1 + 2i\beta)[K] \tag{3}$$

and β is the damping coefficient.

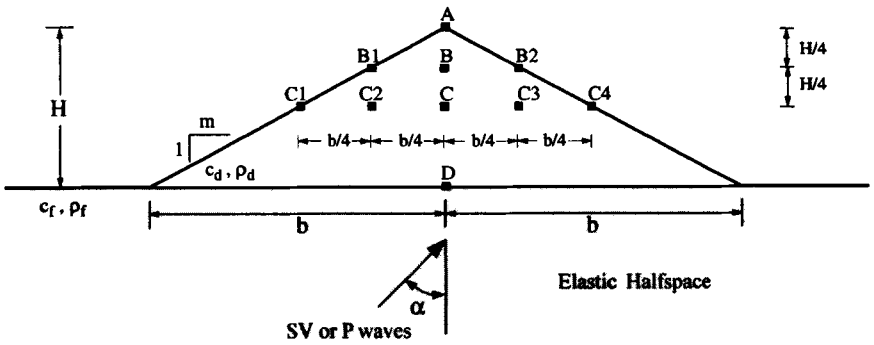

Figure 1. Earth dam cross-section on elastic halfspace subjected to oblique SV or P waves

Boundary element method

Making use of the dynamic reciprocity theorem with one state being the real state of the problem, and the other state being the fundamental singular solution pair expressing the displacement, G_{ij}, and the forces F_{ij}, the frequency-domain governing equation can be expressed in terms of a boundary integral equation as[24]

$$c_{ij}u_j + \int_\Gamma F_{ij}u_j \,\mathrm{d}\Gamma = \int_\Gamma G_{ij}t_j \,\mathrm{d}\Gamma \tag{4}$$

where u and t denote the displacement and traction vectors; $\Gamma = \Gamma_u + \Gamma_t$, in which Γ_u and Γ_t are the boundaries with prescribed displacements and tractions, respectively: and c_{ij} is a constant related to the geometric location and the smoothness of the boundary at the source points. The fundamental solutions G_{ij} and F_{ij} for plane strain steady-state elastodynamics have the form[25]

$$\begin{aligned} G_{ij} &= \frac{1}{2\pi\rho c_2^2}\left[\Phi\delta_{ij} - \Psi r_{,i}r_{,j}\right] \\ F_{ij} &= \frac{1}{2\pi}\left[\left(\frac{\mathrm{d}\Phi}{\mathrm{d}r} - \frac{\Psi}{r}\right)\left(\delta_{ij}\frac{\partial r}{\partial n} + r_{,j}n_{,i}\right)\right. \\ &\quad - 2\frac{\Psi}{r}\left(r_{,i}n_{,j} - 2\frac{\partial r}{\partial n}r_{,i}r_{,j}\right) - 2\frac{\mathrm{d}\Psi}{\mathrm{d}r}\frac{\partial r}{\partial n}r_{,i}r_{,j} \\ &\quad \left. + \left(\frac{c_1^2}{c_2^2} - 2\right)\left(\frac{\mathrm{d}\Phi}{\mathrm{d}r} - \frac{\mathrm{d}\Psi}{\mathrm{d}r} - \frac{\Psi}{r}\right)r_{,i}n_{,j}\right] \end{aligned} \tag{5}$$

where

$$\begin{aligned} \Phi &= K_0\left(\frac{\mathrm{i}\omega r}{c_2}\right) + \frac{c_2}{\mathrm{i}\omega r}\left[K_1\left(\frac{\mathrm{i}\omega r}{c_2}\right) - \frac{c_2}{c_1}K_1\left(\frac{\mathrm{i}\omega r}{c_1}\right)\right] \\ \Psi &= K_2\left(\frac{\mathrm{i}\omega r}{c_2}\right) - \frac{c_2^2}{c_1^2}K_2\left(\frac{\mathrm{i}\omega r}{c_1}\right) \end{aligned} \tag{6}$$

r is the distance between the source and field points, K_0, K_1, K_1 are modified Bessel functions of the second kind, and c_1, c_2 are the P and SV complex valued wave velocities in the elastic body. By discretizing the

boundary of the problem into a finite number of elements and using the same concept of shape functions as in the FEM to describe the nodal displacements, equation (4) can be expressed as a system of linear equations

$$[F]u = [G]t \tag{7}$$

where $[F]$ is the constant coefficient matrix derived by integrating the left hand side of equation (4) and adding c_{ij}; $[G]$ is the coefficient matrix derived by integrating the right-hand side of equation (4). A sufficient portion of the halfspace surface is discretized, so that the error resulting from the approximation is negligible.

Coupled finite element–boundary element formulation

In order to incorporate the wave excitation into the formulation of the coupling procedure, the wave field is divided in two components: (a) the free-field component (superscript f) representing the wave field in an equivalent halfspace having the same material properties and (b) the scattered wave field component (superscript s) due to the existence of geometrical and material irregularities. The displacements can then be expressed as

$$u = u^{\mathrm{f}} + u^{\mathrm{s}} \tag{8}$$

The free-field component can be calculated analytically at all nodes of the near-far field interface, considering the type and angle of the incident wave. Equation (7) can be rewritten as

$$\begin{bmatrix} F_{\mathrm{ii}} & F_{\mathrm{ir}} \\ F_{\mathrm{ri}} & F_{\mathrm{rr}} \end{bmatrix} \begin{bmatrix} u_{\mathrm{i}}^{\mathrm{s}} \\ u_{\mathrm{r}}^{\mathrm{s}} \end{bmatrix} = \begin{bmatrix} G_{\mathrm{ii}} & G_{\mathrm{ir}} \\ G_{\mathrm{ri}} & G_{\mathrm{rr}} \end{bmatrix} \begin{bmatrix} t_{\mathrm{i}} - t_{\mathrm{i}}^{\mathrm{s}} \\ -t_{\mathrm{r}}^{\mathrm{s}} \end{bmatrix} \tag{9}$$

where the subscript i indicates the interaction nodes lying on the FE–BE interface, and the subscript r indicates the rest of the boundary element nodes; $t_{\mathrm{i}}^{\mathrm{s}}$ and $t_{\mathrm{r}}^{\mathrm{s}}$ are stresses due to the scattered wave field, and t_{i} is the stress at the interaction nodes resulting only from the near-field region. The unknowns in equation (9) are the displacement vectors $u_{\mathrm{i}}^{\mathrm{s}}$ and $u_{\mathrm{r}}^{\mathrm{s}}$, and the stress vector t_{i}.

By using the condensation technique, one can eliminate the extra degrees of freedom, keeping only those associated with the interaction nodes. Equation (9) can be expressed as

$$\hat{F}u_{\mathrm{i}}^{\mathrm{s}} = \hat{G}t_{\mathrm{i}} + \hat{C} \tag{10}$$

where

$$\begin{aligned} \hat{F} &= [F_{\mathrm{ii}}] - [F_{\mathrm{ir}}][F_{\mathrm{rr}}]^{-1}[F_{\mathrm{ri}}] \\ \hat{G} &= [G_{\mathrm{ii}}] - [F_{\mathrm{ir}}][F_{\mathrm{rr}}]^{-1}[G_{\mathrm{ri}}] \\ \hat{C} &= -[[G_{\mathrm{ir}}]t_{\mathrm{r}}^{\mathrm{s}} + [G_{\mathrm{ii}}]t_{\mathrm{i}}^{\mathrm{s}}] + [F_{\mathrm{ir}}][F_{\mathrm{rr}}]^{-1}[G_{\mathrm{rr}}]t_{\mathrm{r}}^{\mathrm{s}} \\ &\quad + [F_{\mathrm{ir}}][F_{\mathrm{rr}}]^{-1}[G_{\mathrm{ri}}]t_{\mathrm{i}}^{\mathrm{s}} \end{aligned} \tag{11}$$

To ensure compatibility between the far field discretized with boundary elements and the near field discretized with finite elements, a transformation from BE tractions to FE nodal forces is introduced

$$f_{\mathrm{i}} = -T\,t_{\mathrm{i}} \tag{12}$$

where T is a transformation matrix constructed using the FE shape functions N and the BE shape functions L as

$$T = \int_{\Gamma_{\mathrm{i}}} N^{\mathrm{T}} L \, \mathrm{d}\Gamma_{\mathrm{i}} \tag{13}$$

By making use of equation (12), equation (10) yields

$$\hat{A}u_i^s = -f_i + \hat{B} \tag{14}$$

in which

$$\begin{aligned} \hat{A} &= [T][\hat{G}]^{-1}[\hat{F}] \\ \hat{B} &= [T][\hat{G}]^{-1}[\hat{C}] \end{aligned} \tag{15}$$

The FE system of linear equations (2) can also be written as

$$\begin{bmatrix} A_{dd} & A_{di} \\ A_{id} & A_{ii} \end{bmatrix} \begin{bmatrix} u_d \\ u_i \end{bmatrix} = \begin{bmatrix} f_d \\ f_i \end{bmatrix} \tag{16}$$

where the subscript i indicates the interaction on the BE and FE interface and the subscript d indicates the rest of the FE nodes in the near field.

By combining equations (14) and (16), the complete coupled system takes the form

$$\begin{bmatrix} A_{dd} & A_{di} \\ A_{id} & A_{ii} + \hat{A} \end{bmatrix} \begin{bmatrix} u_d \\ u_i^s \end{bmatrix} = \begin{bmatrix} f_d - A_{di}u_i^f \\ \hat{B} - A_{ii}u_i^f \end{bmatrix} \tag{17}$$

Solution of equation (17) yields the displacements vector u_d in the FE region and the scattering wave field u_i^s at the interaction boundary. The interaction tractions, t_i, the interaction forces, f_i, the scattered wave field, u_r^s and the total displacement field, u, can be calculated using equations (9), (10), (12) and (8), respectively. Information regarding the verification of the presented coupled FE–BE formulation may be found in Reference 22.

RESPONSE OF EARTH DAMS TO SV AND P WAVES

The general formulation presented above is now applied to study the effects of the foundation flexibility and the spatial variability of the ground motion on the response of infinitely long earth dams. The dam body consists of a linearly hysteretic elastic material and is founded on an elastic halfspace (Figure 1). The excitation consists of harmonic obliquely incident SV and P waves travelling across the width of the dam cross-section.

Two dams having the same height of $H = 100$ m and symmetric slopes of 2:1 and 3:1, respectively, are considered. The dam material has an elastic Young's modulus $E_d = 8{\cdot}19 \times 10^5$ kN/m^2, mass density $\rho_d = 1920$ kg/m^3, Poisson's ratio $\nu_d = 1/3$, shear wave velocity $c_d = 400$ m/s and damping ratio $\beta_d = 10$ per cent. The foundation material has a mass density $\rho_f = 2400$ kg/m^3, Poisson's ratio $\nu_f = 1/3$ and no material damping. The flexibility of the foundation is considered by examining a range of impedance ratio values, defined as

$$\mathrm{IR} = \frac{\rho_f c_f}{\rho_d c_d} \tag{18}$$

where c_f is the shear wave velocity of the foundation material. The dam body is discretized using four-node plane strain isoparametric elements, whereas the half-space is discretized using two-node boundary elements. The discretized length of the half-space surface is taken equal to five times the dam base width.

For harmonic SV and P wave excitation, the results of the parametric study are presented in the following in terms of steady-state amplifications, AF, of the motion within the dam body with respect to the free-field surface motion, i.e.,

$$\mathrm{AF} = \left| \frac{u_d(\omega)}{u_g} \right| \tag{19}$$

where $u_d(\omega)$ = total displacement in the dam; u_g = horizontal free-field motion for the case of incident SV waves or vertical free-field motion for the case of incident P waves; and ω is the frequency of the incident waves. In the following, AF is plotted versus a dimensionless frequency, a_0, equal to

$$a_0 = \frac{\omega H}{c_d} \tag{20}$$

Due to space limitations, only a part of the results is presented here, referring mainly to the dam with slopes 2:1. However, the discussion and conclusions reflect the results from all analyses made. More information for the rest of the analyses for both harmonic and transient excitation may be found in Reference 22.

Effect of impedance ratio

It is of interest to examine first the effect of the flexibility of the elastic rock halfspace on the dam response. Figure 2 shows the first ten vibrational modes and the dimensionless natural frequencies of the dam having slopes 2:1, assuming rigid base (IR = ∞). For this dam, Figure 3 shows the steady-state amplification, AF, of the horizontal motion at the points A, B, B1, C, C1, C2 and D, due to vertically incident SV waves. The five curves in each plot correspond to impedance ratios IR = 2, 3, 5, 10 and ∞. The results demonstrate that the flexibility of the base rock has a substantial effect on the dam response near the first resonance in shear vibration, occurring at $a_0 \approx 2{\cdot}2$ for IR = ∞. More specifically, AF at first resonance is equal to 8·5 for IR = ∞, 7·3 for IR = 10, 5·6 for IR = 5, 3·6 for IR = 3 and 2·3 for IR = 2. For higher frequencies,however, the effect of the foundation flexibility becomes significantly smaller. Furthermore, the response near the crest and within the dam body becomes also smaller.

Higher resonances in shear vibration include also rocking motion, more evident near the upper part of the dam. For example, at point A, the small peak at $a_0 \approx 3{\cdot}8$ corresponds to resonance mainly in rocking vibration, whereas the peak at $a_0 \approx 5$ corresponds to resonance mainly in shear vibration. The peak at $a_0 \approx 8$ is the combined effect of three adjacent shear-rocking vibrational modes.

At the lower half of the dam body and away from the slopes, deamplification of the motion is observed. At the dam base (point D), this deamplification becomes more significant as IR decreases, especially at first resonance. Near the slopes (point C1), the second resonance peak is significant.

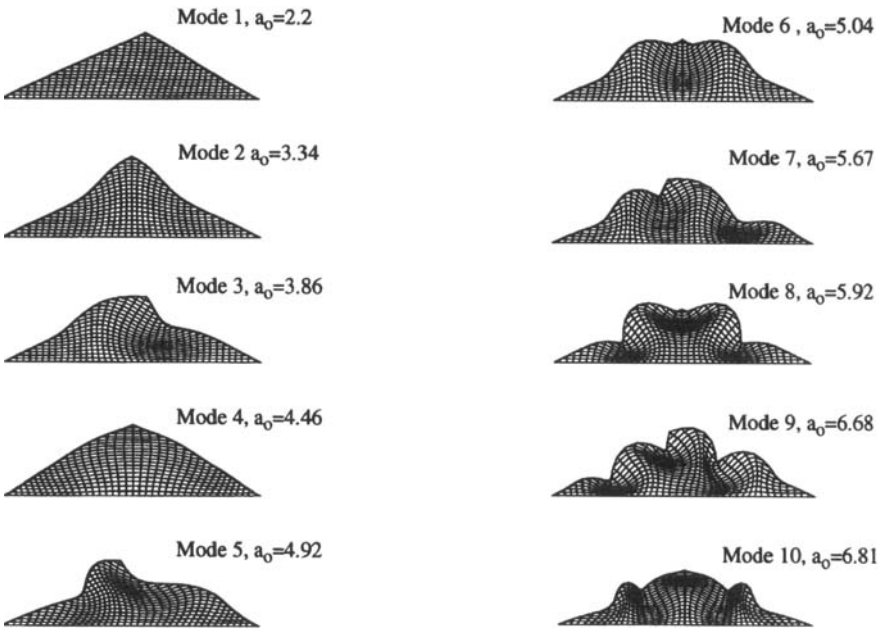

Figure 2. The first ten vibrational modes of the dam with slopes 2:1 founded on rigid base

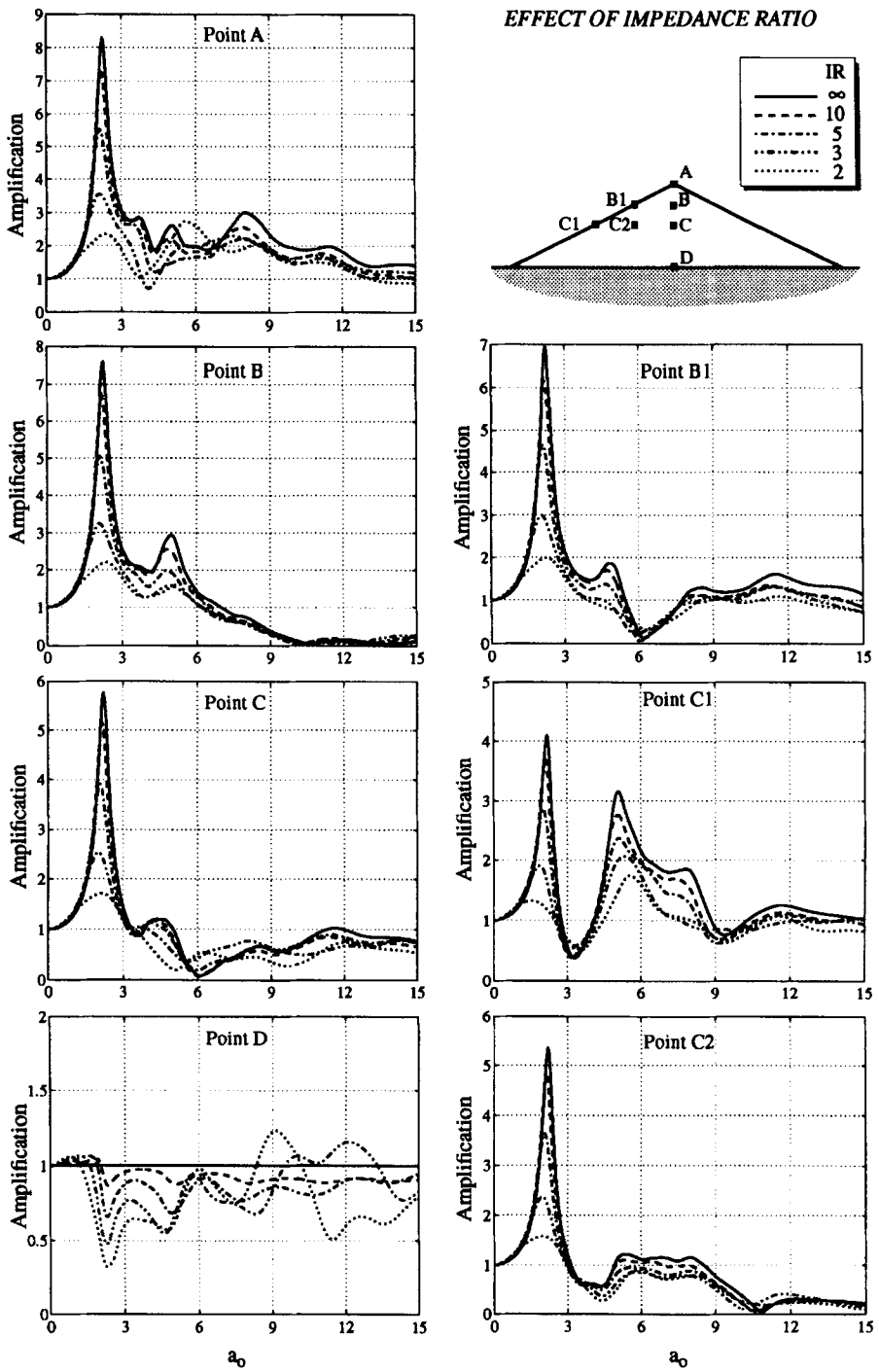

Figure 3. Steady-state horizontal amplification at various points within the dam body for vertically incident SV waves and impedance ratios IR = 2, 3, 5, 10, and ∞. (Dam slope 2:1)

Figure 4 shows the amplification, AF, of the horizontal motion due to vertically incident SV waves for the dam with slopes equal to 3:1. The results indicate more or less the same trends shown in Figure 3 regarding the effect of flexibility on the dam response. However, as the slopes become flatter, the response of the dam tends to be more in shear rather than in rocking vibration. Indeed, the rocking resonance peak observed at $a_0 \approx 3{\cdot}8$ in Figure 3 does not appear in Figure 4. Some difference is also observed in the response near the slopes, which seems to be more pronounced at the second natural frequency in shear vibration for the flatter slope dam (point C1).

It is interesting to compare the amplification results in Figures 3 and 4 with those from the plane strain shear beam (SB) model on elastic foundation. The latter assumes that the response of a dam to vertically incident SV waves is only in horizontal lateral shear deformation with the upstream–downstream displacements uniformly distributed across the dam width. The steady-state amplification AF at a depth z from the crest is given by

$$\mathrm{AF} = \left| \frac{J_0\left(a_0^* \frac{z}{H}\right)}{J_0(a_0^*) + \mathrm{i}\frac{\sqrt{1 + 2\mathrm{i}\beta_d}}{\mathrm{IR}} J_1(a_0^*)} \right| \tag{21}$$

where

$$a_0^* = \frac{a_0}{\sqrt{1 + 2\mathrm{i}\beta_d}} \tag{22}$$

J_n is the Bessel function of first kind and order n and $i = \sqrt{-1}$. Figure 5 shows the AF evaluated from equation (21) at the points A, B, C, and D. Notice that, at the first resonance, there is very good agreement between the results from equation (21) and those of Figures 3 and 4 from the more rigorous FE–BE analysis. For higher frequencies, however, the shear beam predicts sharper resonance peaks at the crest (point A) compared to those from the FE–BE method. At points lower than the crest area, the agreement between the FE–BE and SB results for the first and higher natural frequencies is very good (e.g. compare the AF at points B and C2 from Figures 3 and 4, with AF at points B and C in Figure 5). The differences in the response obtained from the two methods are explained mainly by the fact that the SB assumes response only in shear and ignores the SV wave reflections and generation of P waves along the dam slopes.

Figure 6 shows the steady-state amplification AF of the vertical motion at the same points within a dam having slopes 2:1 and subjected to vertically incident P waves. As in the case of SV waves, the flexibility of the base rock has a substantial effect on the dam response near the first resonance in vertical vibration. More specifically, AF is equal to 6·2 for IR = ∞, 6 for IR = 10, 4·9 for IR = 5, 3·3 for IR = 3 and 2·2 for IR = 2. For higher frequencies, the response near the crest and within the dam body is smaller compared to that at first resonance. The effect of the flexible base is also smaller at higher frequencies, but greater than that observed in the case of SV waves in Figure 3. At the lower half of the dam body and away from the slopes, deamplification of the motion at high frequencies takes place. At the dam base (point D), this deamplification of the motion is substantial at first resonance. Near the slopes (points B1, C1 and C2), AF at the second resonance is significant. For the dam having slopes equal to 3:1, the results regarding the effect of the base flexibility indicate similar trends as those shown in Figure 5, with a slight reduction in the AF at first resonance. More striking is the difference observed in the response near the slopes, which becomes maximum at the second natural frequency in vertical vibration for the flatter slope dam.

Figure 7 plots the amplitude of the crest amplification at first resonance versus the inverse of the impedance ratio (1/IR) for the two dams. The upper shaded area represents the crest amplification for vertically propagating SV waves, whereas the lower shaded area represents the crest amplification for vertically propagation P waves. For each case, the upper bound of the shaded area corresponds to the steeper dam and the lower bounds to the flatter dam. The dashed curve represents the crest amplification obtained from the solution of the shear beam on flexible halfspace, given by equation (21). Figure 7 demonstrates that

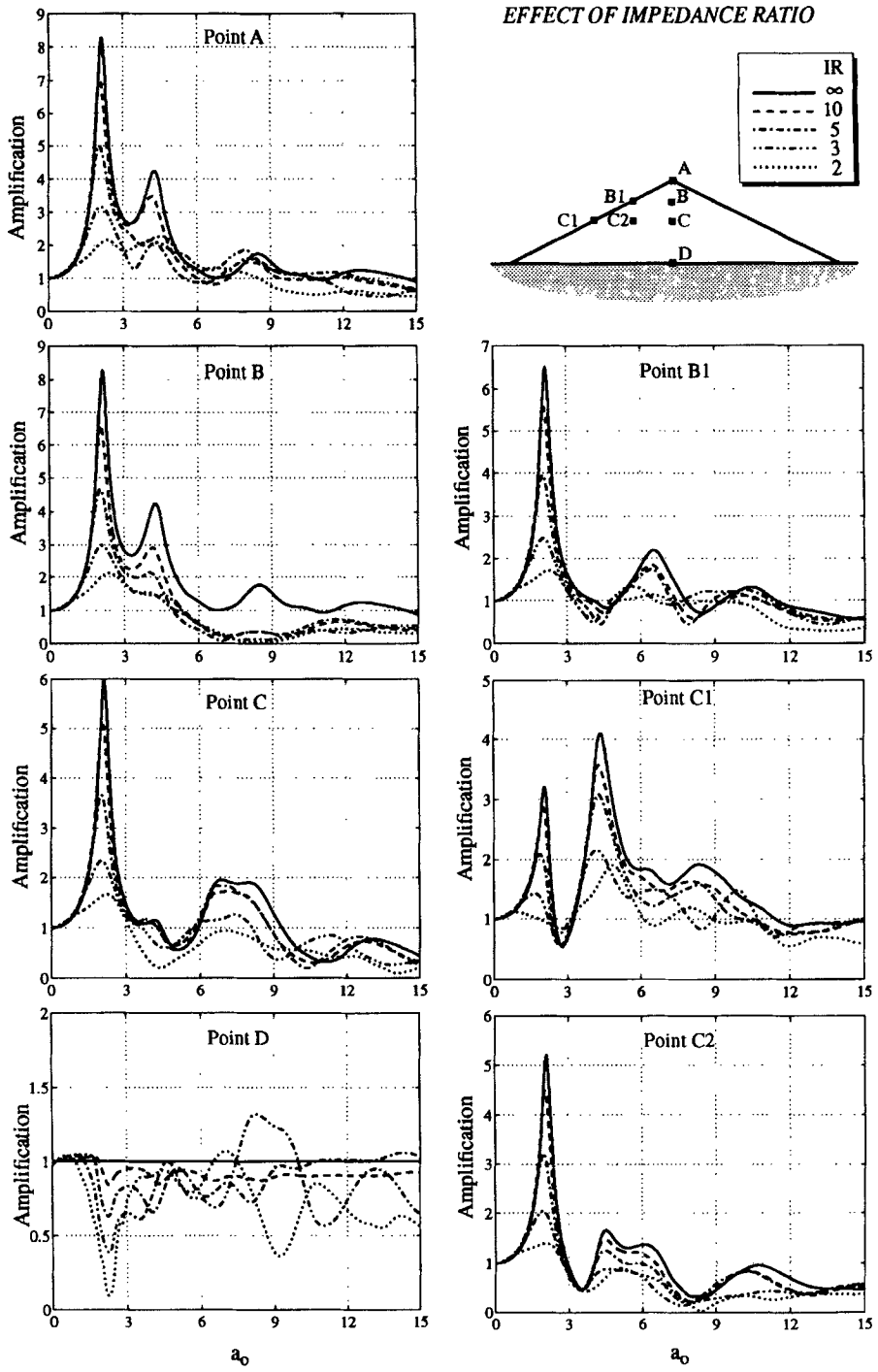

Figure 4. Steady-state horizontal amplification at various points within the dam body for vertically incident SV waves and impedance ratios IR = 2, 3, 5, 10, and ∞. (Dam slope 3:1)

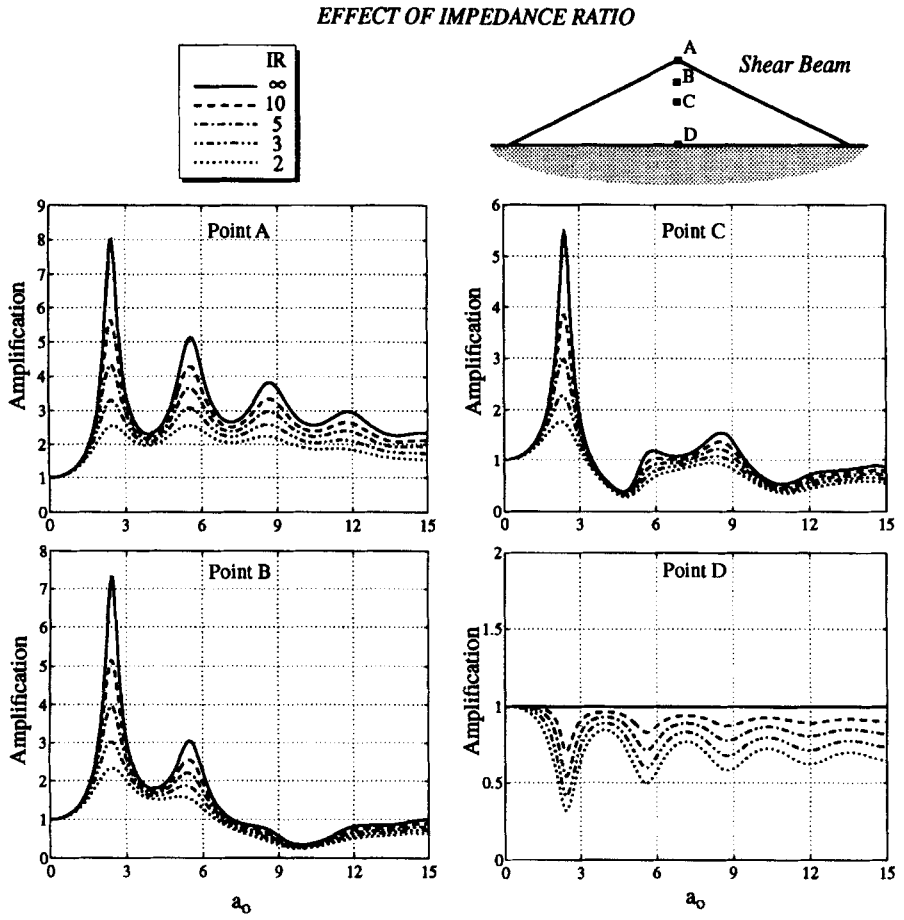

Figure 5. Steady-state horizontal amplification at various points within the dam body obtained from the Shear Beam model for vertically incident SV waves and impedance ratios IR = 2, 3, 5, 10, and ∞

IR has a significant effect on AF and that this effect is generally larger for the shear-rocking vibration than for the vertical (compression–extension) vibration. However, for a typical practical range of IR values between 2 and 8, the amplification results from all analyses using the rigorous FE–BE method and the simplified shear beam model are in fairly close agreement.

Effect of the angle of incidence

The effect of the spatial variability of the ground motion is examined in Figures 8–11, which present the horizontal and vertical amplification AF for obliquely incident SV and P waves at various angles α. The figures show the response at points A, B1, B2, C1, C2, C3, and C4 of a dam having impedance ratio IR = 5 and slopes 2:1.

Figures 8 and 9 show the amplification AF of the horizontal and vertical motion, respectively, for SV waves incident at angle $\alpha = 0$, 15 and 30°. The horizontal response corresponding to different angles of incidence seems to be in good agreement for all points within the dam body. Such agreement suggests that the spatial variability of the ground motion across the dam base induced by oblique SV waves has relatively small effect on the horizontal motion within the dam body. Similar trends are also shown for the dam with slopes 3:1.[22] The amplification AF induced in the vertical direction is several times smaller than the AF in the horizontal direction. For vertically incident SV waves ($\alpha = 0°$), due to the anti-symmetry of the loading,

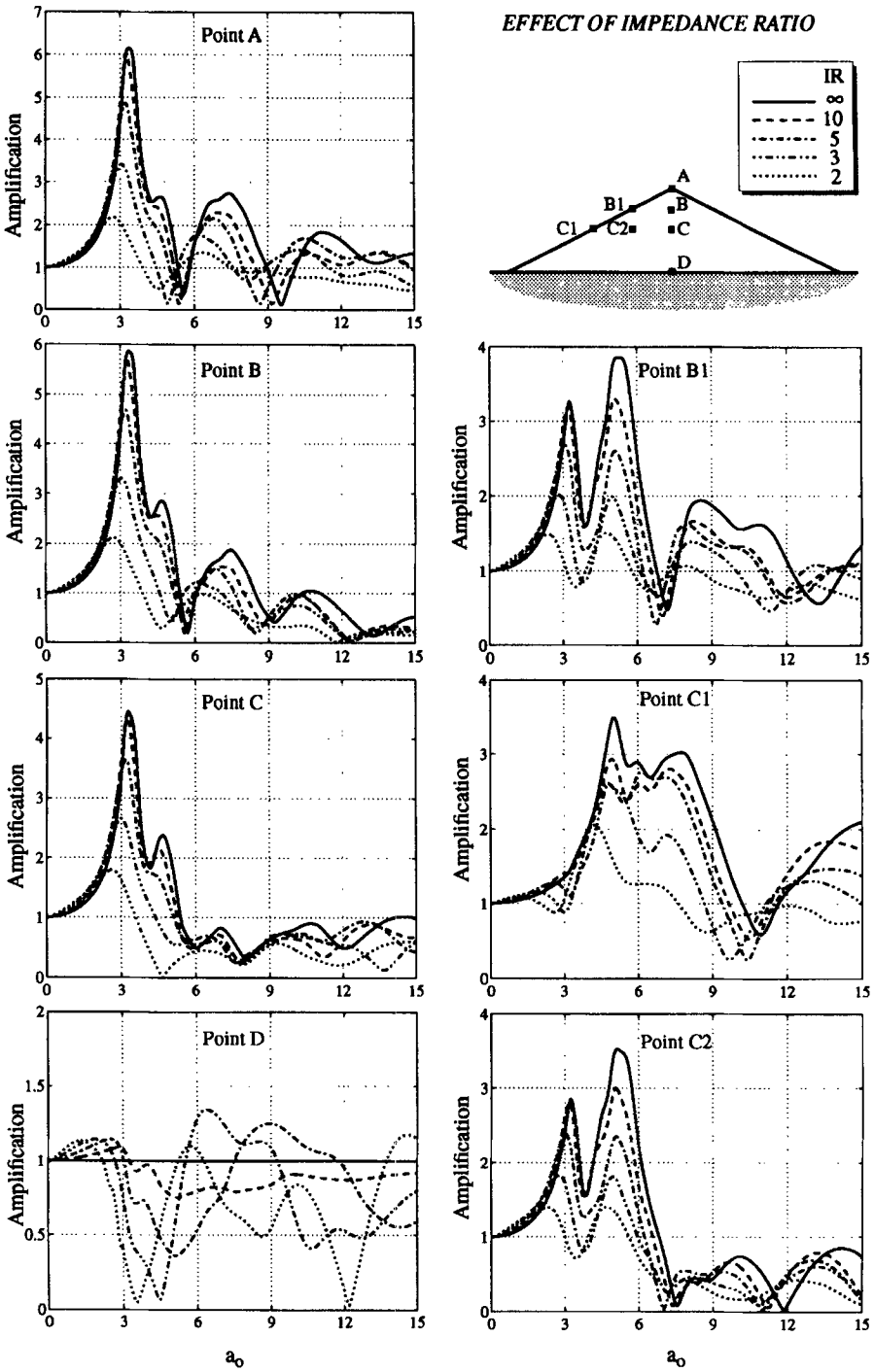

Figure 6. Steady-state vertical amplification at various points within the dam body for vertically incident P waves and impedance ratios IR = 2, 3, 5, 10, and ∞. (Dam slope 2:1)

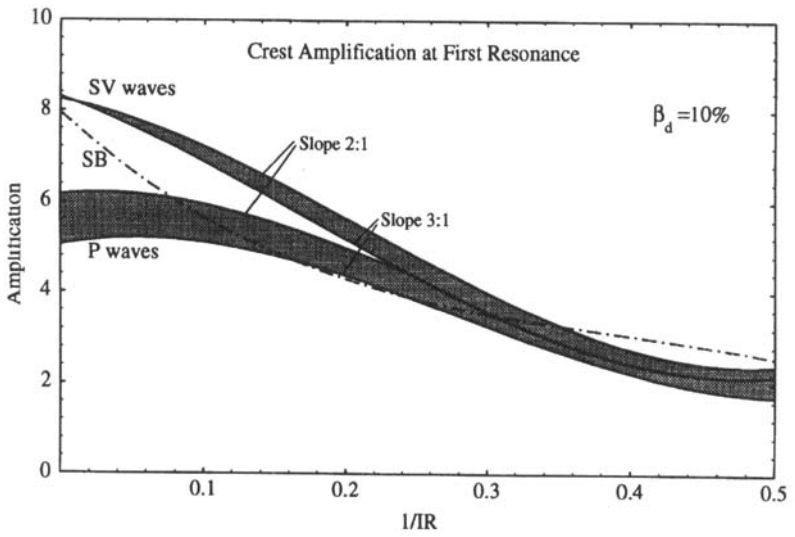

Figure 7. Maximum crest amplification at first resonance versus the inverse of the impedance ratio. (Material damping $\beta_d = 10\%$)

the vertical response along the central axis of the dam cross-section is equal to zero. For the rest of the dam body, the vertical response is only a fraction of the horizontal one, because the dam deforms mainly in shear. For obliquely incident waves, the differences in the vertical motion induced at the left and right sides of the dam cross-section are shown at the pair points B1–B2, C1–C4, and C2–C3 in Figure 9. However, again, the overall vertical response is only a fraction of the horizontal response. Indeed, for $\alpha = 30°$, the maximum horizontal amplification at crest is about 5·5, whereas the maximum vertical amplification is equal to 1·4. The small amplitude of the vertical response may be explained if one considers that when an SV wave of amplitude A_i impinges at an angle $\alpha = 30°$ at the dam–foundation interface, the transmitted SV wave has an amplitude of about 2 A_i and forms an angle of 7° to the vertical, whereas the transmitted P wave has an amplitude of only $0{\cdot}14A_i$. Although the total motion at the dam-foundation interface includes additional waves returning from complex reflection paths within the dam body, the presence of almost vertically transmitted high-amplitude SV waves and small-amplitude P waves can explain the significant lateral and small vertical response.

Figures 10 and 11 plot the amplification AF of the vertical and horizontal motion, respectively, for the same dam subjected to P waves incident at angles $\alpha = 0$, 15, 30 and 45°. As in the case of SV waves, the results for the P waves suggest that the spatial variability of the ground motion across the dam base has relatively small effect on the vertical motion. In contrast, the amplification AF of the horizontal motion shown in Figure 11 demonstrates that the amplification in the horizontal direction increases significantly as the angle of incidence of the P waves increases from $\alpha = 0$ to 45°. Indeed, as α increases there is a significant resonance peak of the horizontal amplification consistently at $a_0 \approx 2{\cdot}1$, which corresponds to the first resonance in shear vibration for IR = 5. Notice that for $\alpha = 45°$ the horizontal crest amplification is about 4·65, i.e. almost as high as the maximum vertical amplification, which is equal to 4·85. The presence of such high horizontal response can be explained if one considers that when a P wave of amplitude A_i impinges at an angle $\alpha = 45°$ at the dam–foundation interface, the resulting refracted P wave has an amplitude of about A_i and forms an angle of 10° to the vertical, whereas the refracted SV wave has an amplitude of $0{\cdot}89A_i$ and forms an angle of 5° to the vertical. The presence of a high amplitude obliquely transmitted SV wave can explain the significant horizontal shear response and its dependence on the angle of incidence. Similar trends are also observed in the response of the flatter dam.[22]

The above results demonstrate that P waves, incident at angle $\alpha \geqslant 30°$ and travelling across the dam width, may induce horizontal response that is particularly strong for frequencies near the first resonance in shear

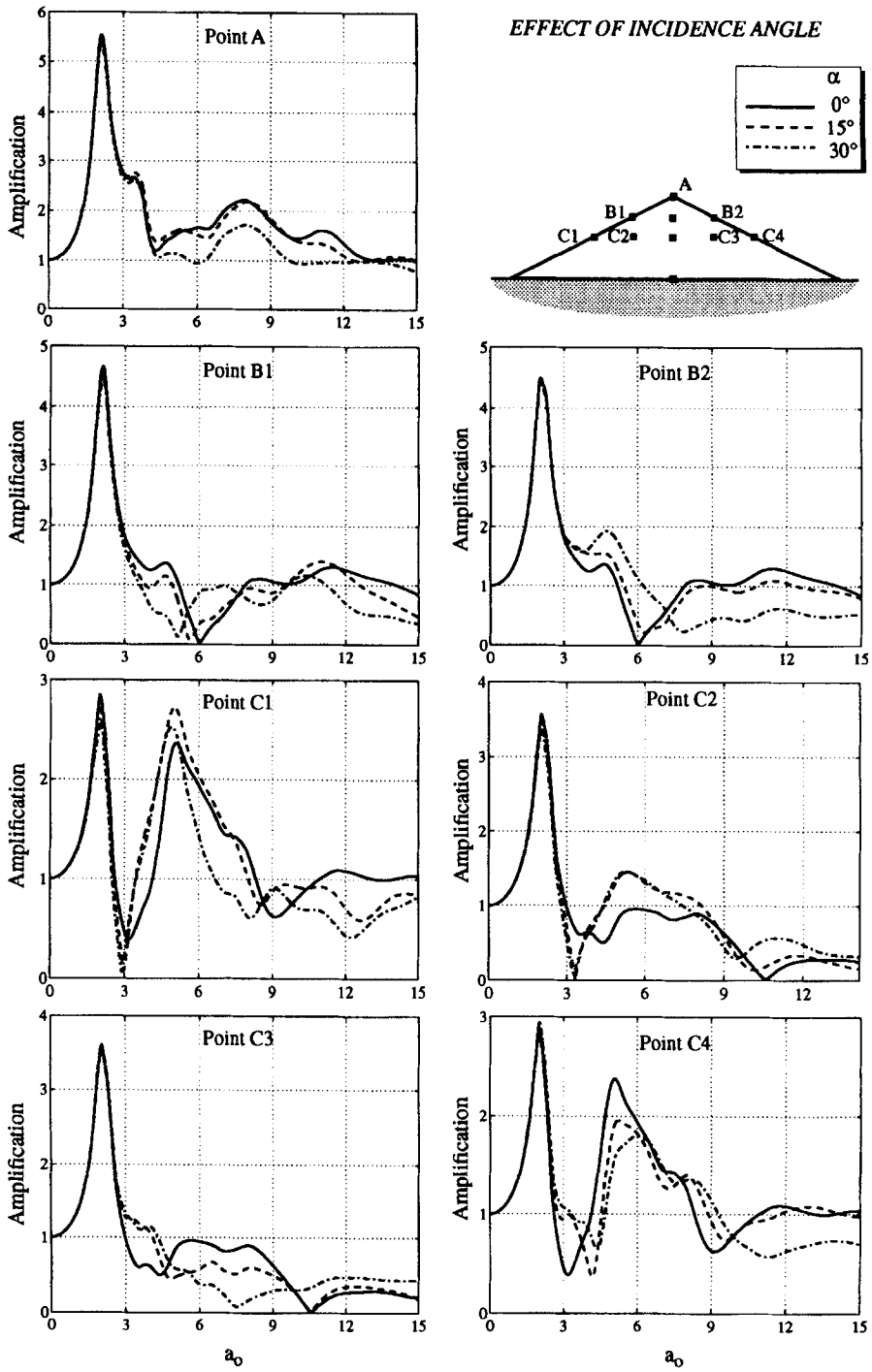

Figure 8. Steady-state horizontal amplification at various points within the dam subjected to obliquely incident SV waves at angles $\alpha = 0°$, 15° and 30°. (Impedance ratio IR = 5; dam slope 2:1)

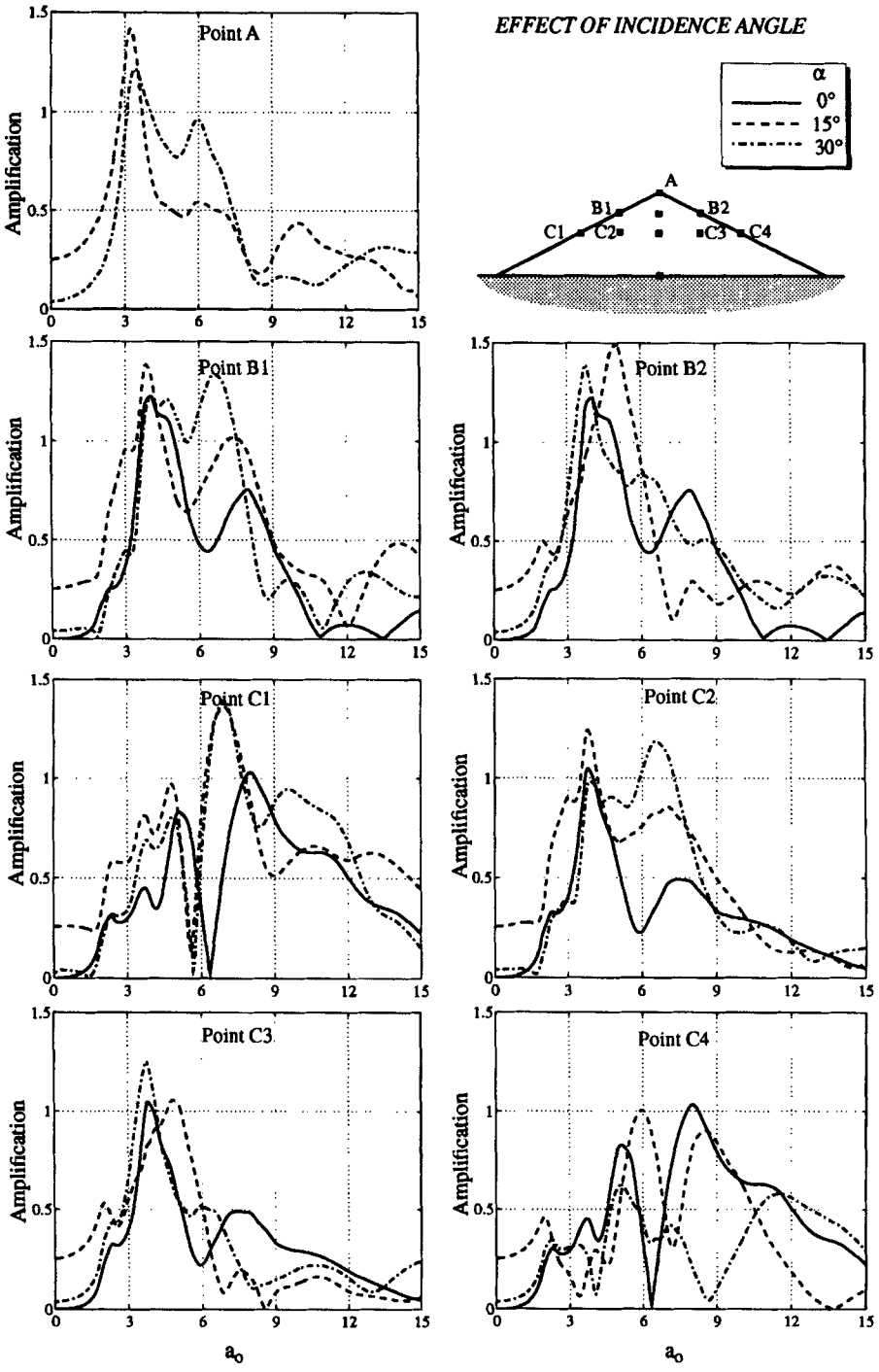

Figure 9. Steady-state vertical amplification at various points within a dam subjected to obliquely incident SV waves at angles $\alpha = 0°$, 15° and 30°. (Impedance ratio IR = 5; dam slope 2:1)

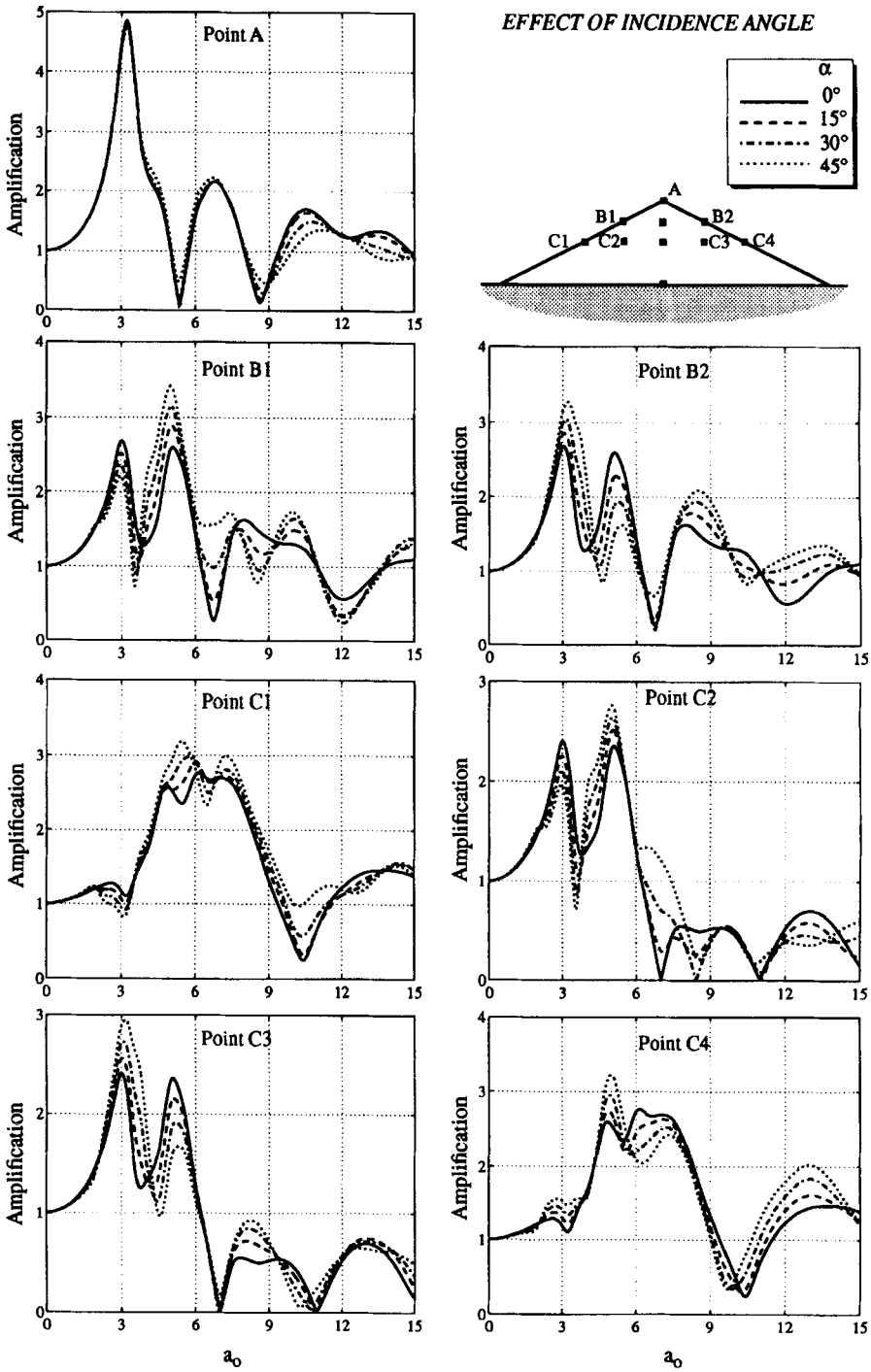

Figure 10. Steady-state vertical amplification at various points within the dam subjected to obliquely incident P waves at angles $\alpha = 0°$, 15°, 30° and 45°. (Impedance ratio IR = 5; dam slope 2:1)

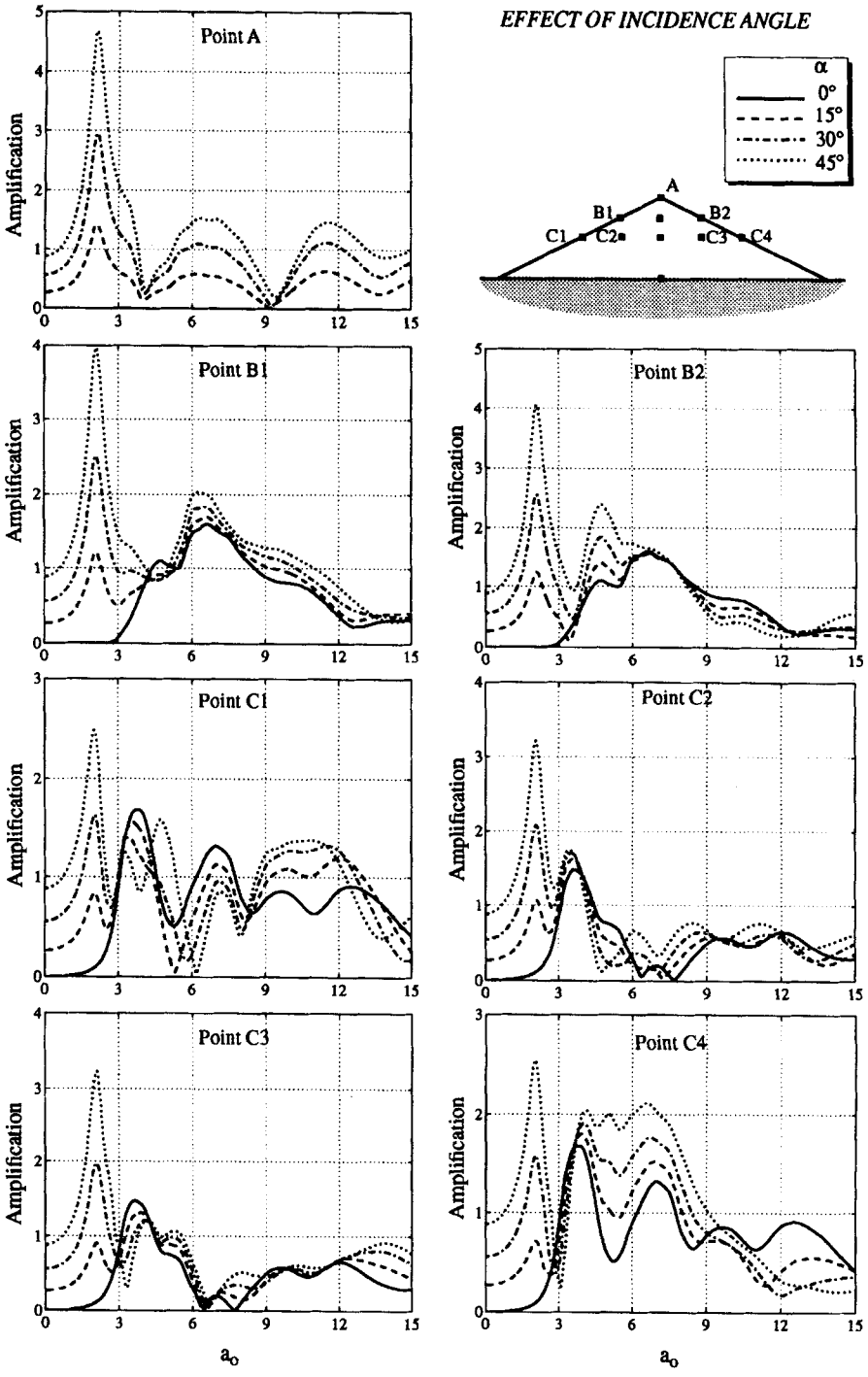

Figure 11. Steady-state horizontal amplification at various points within a dam subjected to obliquely incident P waves at angles $\alpha = 0°$, 15°, 30° and 45°. (Impedance ratio IR = 5; dam slope 2:1)

vibration. This additional horizontal response is caused by the spatial variability of the ground motion, which may induce antisymmetric (or, in general, asymmetric) vibrational modes that do not appear in the case of vertically incident waves ($\alpha = 0°$). The conclusion that the response of a dam to a spatially variable motion may be substantially higher than that obtained for a space-invariant motion, drawn from this study, is in agreement with the conclusion drawn from the earlier studies[3,4] that did not consider the dam–foundation interaction. Furthermore, it is in agreement with the conclusions from similar studies considering SH waves propagating along the longitudinal direction of symmetric dams in semicircular, semielliptical and rectangular canyons. The latter studies have also shown that, even at small incidence angles, oblique waves induce additional 'antisymmetric' vibrational modes, which may lead to substantially higher response in the dam than the response caused by vertically propagating waves.[6–8]

In reality, a seismic event experienced by a dam body on a homogeneous half-space may consist of P, S and Rayleigh waves. To different degrees each of these waves may significantly increase the dam response due to the spatial variability of the ground motion, depending on the magnitude of the earthquake, the distance and depth of the source, etc. Rayleigh waves are expected to have a particularly significant effect in increasing the dam response, because these waves transfer a substantial amount of energy and travel in the horizontal direction along the surface of the half-space, thereby, increasing the spatial variability of the ground motion.

CONCLUSIONS

A hybrid numerical formulation combining the Finite Element and the Boundary Element methods has been used to study the effects of dam–foundation interaction on the response of earth dams subjected to obliquely incident P and SV waves. The developed hybrid method was proven to be very powerful and could be used to solve accurately and efficiently soil–structure interaction problems of complex geometry and material heterogeneity. The two-dimensional frequency-domain formulation has been used here to investigate the response of long dams to SV and P waves travelling across the width of the dam, assuming linear hysteretic soil behaviour.

The results showed the significant effect of the flexibility of the foundation rock in reducing the overall response of the dam, by accounting rigorously for the energy radiated back into the half-space. These effects are particularly significant near the first resonance. For a typical range of impedance ratio values between 2 to 8, the amplification results from all analyses using the rigorous FE–BE method and the simplified shear beam model are in fairly close agreement.

The effect of the spatial variability of the ground motion for SV waves travelling across the width of the dam seem to be relatively small for angles of incidence $\alpha \leqslant 30°$. In contrast, the effects of the spatial variability of the ground motion for P waves increase significantly as the angle of incidence increases from $\alpha = 0$ to 45°. The response increases mainly in the horizontal direction due to the excitation of additional vibrational modes that do not appear in the case of vertically incident waves. The conclusion of this study, that the response of a dam to a spatially variable motion may be substantially higher than that caused by vertically propagating waves, is in agreement with findings from the earlier studies[3,4] that did not consider the dam–foundation interaction and from more recent studies considering SV waves propagating along the longitudinal direction of symmetric dams in semicircular, semielliptical and rectangular canyons.[6–8]

REFERENCES

1. G. Gazetas, 'Seismic response of earth dams: some recent developments', *J. soil dyn. earthquake eng.* **6**, 1–47 (1987).
2. G. Gazetas and P. Dakoulas, 'Seismic analysis and design of rockfill dams: state-of-the art', *J. soil dyn. earthquake eng.* **11**, 27–61 (1992).
3. A. K. Chopra, M. Dibaj, R. W. Clough, J. Penzien and H. B. Seed, 'Earthquake analysis of earth dams', *Proc. 4th world conf. earthquake engineering*, Santiago, 1969.
4. M. Dibaj and J. Penzien, 'Response of earth dams to traveling seismic waves', *J. soil mech. found. div. ASCE* **95**, 541–560 (1969).
5. T. M. Nahhas, 'Dynamics of earth dams', *Ph.D. thesis*, University of Southern California, Los Angeles, CA, 1987.
6. P. Dakoulas and Hsu, 'Response of earth dams in semi-elliptical flexible canyons to oblique SH waves', *J. eng. mech. ASCE* **121**, 379–391 (1995).
7. P. Dakoulas, 'Response of earth dams in semi-cylindrical valleys subjected to plane SH waves', *J. eng. mech. ASCE* **119**, 74–90 (1993).

8. P. Dakoulas, 'Earth dam–canyon interaction effects for obliquely incident SH waves', *J. geotechn. eng. div. ASCE* **119**, 1696–1716 (1993).
9. P. Dakoulas, and H. Hashmi, 'Wave passage effects on the response of earth dams', *J. soils found.* **32**, 97–110 (1992).
10. O. C. Zienkiewicz, D. M. Kelly and P. Bettes, 'The coupling of the finite element method and the boundary solution procedures', *Int. j. numer. methods eng.* **1**, 355–376 (1977).
11. C. A. Brebbia, J. C. F. Telles and L. C. Wrobel, *Boundary Element Techniques*, Springer, Berlin, 1984.
12. D. E. Beskos, 'Boundary element methods in dynamic analysis', *Appl. mech. rev.* **40**, 1–23 (1987).
13. S. Kobayashi and K. Mori, 'Three dimensional dynamic analysis of soil-structure interaction by boundary integral equation-finite element combined method', in *Innovative Numerical Methods in Engineering*, Springer, Berlin, 1986, pp. 613–618.
14. S. Wang, 'Coupled boundary and finite elements for dynamic structure (3D)-foundation-soil interaction', *Comput. struct.* **44**, 807–812 (1992).
15. L. Auersch and G. Schmid, 'A simple boundary element formulation and its application to wavefield excited soil-structure interaction', *Earthquake eng. struct. dyn.* **19**, 931–947 (1990).
16. J. Bielak, R. C. MacCamy, D. S. McGhee and A. Barry, 'Unified symmetric BEM-FEM for site effects on ground motion-SH waves', *J. eng. mech. ASCE* **117**, 2265–2285 (1991).
17. C. Zhang, O. A. Pekau and J. Feng, 'Application of FE–BE–IBE coupling to dynamic interaction between alluvial soil and rock canyons', *Earthquake eng. struct. dyn.* **21**, 367–385 (1992).
18. T. K. Mossessian and M. Dravinski, 'Application of hybrid method for scattering of P, SV, and Rayleigh waves by near-surface irregularities', *Bull. seism. soc. Am.* **77**, 1784–1803 (1987).
19. C. C. Spyrakos and D. E. Beskos, 'Dynamic response of flexible strip-foundations by boundary and finite elements', *Soil dyn. earthquake eng.* **5**, 84–96 (1986).
20. D. L. Karabalis and D. E. Beskos, 'Dynamic response of 3-D flexible foundations by time domain BEM and FEM', *Soil dyn. earthquake eng.* **4**, 91–101 (1985).
21. O. Von Estorff and E. Kausel, 'Coupling of boundary and finite elements for soil–structure interaction problems', *Earthquake eng. struct. dyn.* **18**, 1065–1075 (1989).
22. H. Abouseeda, 'A hybrid finite element–boundary element method for linear and nonlinear analysis of earth dams', *Ph.D. thesis*, Rice University, Houston, Texas, 1996.
23. O. C. Zienkiewicz, *The Finite Element Method*, 3rd edn, McGraw-Hill, New York, 1977.
24. A. C. Eringen and E. S. Suhubi, *Elastodynamics*, Vol. II, Academic Press, New York, 1975.
25. T. A. Cruse and F. J. Rizzo, 'A direct formulation and numerical solution of the general transient elastodynamic problem. 1', *Int. j. math. anal. appl.* **22**, 244–259 (1968).